Cross-Linking Chitosan Nanofibers

Jessica D. Schiffman and Caroline L. Schauer*

Department of Materials Science and Engineering, Drexel University, Philadelphia, Pennsylvania 19104

Received August 17, 2006; Revised Manuscript Received October 27, 2006

In the present study, we have electrospun various grades of chitosan and cross-linked them using a novel method involving glutaraldehyde (GA) vapor, utilizing a Schiff base imine functionality. Chemical, structural, and mechanical analyses have been conducted by Fourier transform infrared spectroscopy (FTIR), scanning electron microscopy (SEM), and Kawabata microtensile testing, respectively. Additionally, the solubilities of the as-spun and cross-linked chitosan mats have been evaluated;solubility was greatly improved after cross-linking. SEM images displayed evidence that unfiltered low, medium, and high molecular weight chitosans, as well as practical-grade chitosan, can be electrospun into nanofibrous mats. The as-spun medium molecular weight chitosan nanofibers have a Young's modulus of 154.9 ± 40.0 MPa and display a pseudo-yield point that arose due to the transition from the pulling of a fibrous mat with high cohesive strength to the sliding and elongation of fibers. As-spun mats were highly soluble in acidic and aqueous solutions. After cross-linking, the medium molecular weight fibers increased in diameter by an average of 161 nm, have a decreased Young's modulus of 150.8 ± 43.6 MPa, and were insoluble in basic, acidic, and aqueous solutions. Though the extent to which GA penetrates into the chitosan fibers is currently unknown, it is evident that the cross-linking resulted in increased brittleness, a color change, and the restriction of fiber sliding that resulted in the loss of a pseudo-yield point.

Introduction

Chitin is a nitrogen-rich polysaccharide derived from crustaceans, mollusks, insects, and fungi; it is the second most abundant organic material (produced by biosynthesis) after cellulose.[1] It is a high molecular weight (MW) linear polymer composed of *N*-acetyl-D-glucosamine (*N*-acetyl-2-amino-2-deoxy-D-glucopyranose) units linked by β-D-(1 → 4) bonds. Chitosan is the N-deacetylated derivative of chitin; however, the deacetylation process is rarely complete. A sharp nomenclature difference between chitin and chitosan based on the degree of N-deacetylation has never been precisely defined; commercial chitosan typically is ∼85% deacetylated.[1] Defining the molecular weight of chitosan, or any naturally occurring polysaccharide, has historically been difficult. This is true for chitosan in particular because its backbone of (1 → 4)-β-D-glucosamine residues is randomly acetylated. Additionally, due to purification challenges, all natural polymers experience batch-to-batch variation.[2] Therefore, chitosan is a general term applying to many deacetylated chitins having a variety of optical characteristics, crystallinity, degree of acetylation, impurity content, and molecular weights.

As a natural polymer, chitosan intrinsically exhibits enticing properties such as biocompatibility, biodegradability, and aqueous adsorption capabilities. These properties make chitosan an ideal polymer for a wide variety of fields and industrial applications including textiles,[3] ophthalmology,[1] paper coatings,[4] medical,[5−7] agricultural,[8] and food.[9,10] However, processing chitosan can be challenging due to its tendency to coagulate with proteins at high pH, its insolubility in most solvent systems including water, and its high solution viscosity. Chitosan is known to be soluble in dilute organic acids[11] such as acetic, formic, succinic, lactic, and malic acids.

The amine of chitosan can be used to cross-link the polymer by use of a variety of cross-linkers, including diisocyanates, Resimene,[12] *N*,*N*-disuccinimidyl suberate,[13] epichlorohydrin,[14] gepinin,[15] and hexamethylene 1,6-di(aminocarboxysulfonate).[16,17] Glutaraldehyde (GA) has also been demonstrated to cross-link chitosan[18−21] through a number of proposed mechanisms. The first is by Michael-type adducts with terminal aldehydes, which lead to the formation of carbonyl groups (Scheme 1, right).[19,22] The second main cross-linking method, Schiff base formation, leads to imine-type functionality (Scheme 1, left).[23] In our experiments, we utilize GA vapor to cross-link chitosan fibers and observe Schiff base formation as reported previously in the literature.[19,23,24]

Electrospinning creates nonwoven fiber mats, with larger specific surface areas and smaller pores than conventional methods of fiber production, by utilizing electrostatic forces to create fibers; conventional methods such as melt spinning, dry spinning, and wet spinning rely on mechanical forces to produce fibers.[25] In the electrospinning process, a polymer solution is advanced through a syringe with a needle on the end to form a Taylor cone (a conically shaped volume of fluid). A voltage drop is created between the needle and collector.[26] When the electrostatic force is able to overcome the surface tension force, and a thin jet will form and thin out over the course of three stages: jet initiation and extension in a straight line, whipping instability, and jet solidification and fiber collection.[26] Electrospun nanofibers have potential uses in a variety of industries such as medicine, packaging, agriculture, and automotive, with specific applications including air filtration, protective clothing, substitutes for agricultural pesticides, and nanocomposites.[27]

Most of the previous research involving the electrospinning of chitosan has focused on using weak acetic acid solutions or creating matrix polymer fibers consisting of chitosan and another polymer, such as poly(ethylene oxide) (PEO).[28−31] Min et al.[32] created chitosan nanofibers by first electrospinning chitin nanofibers with 1,1,1,3,3,3-hexafluoro-2-propanol (HFIP) as the solvent, followed by deacetylation of the as-spun chitin fibers with NaOH at various temperatures. Ohkawa et al.[33] have

* Corresponding author: e-mail cschauer@cbis.ece.drexel.edu.

10.1021/bm060804s CCC: $37.00
Published on Web 12/30/2006

Scheme 1. Glutaraldehyde Cross-Links Chitosan either by a Schiff Base Imine Functionality (left) and/or by Michael-type Adducts with Terminal Aldehydes (right)

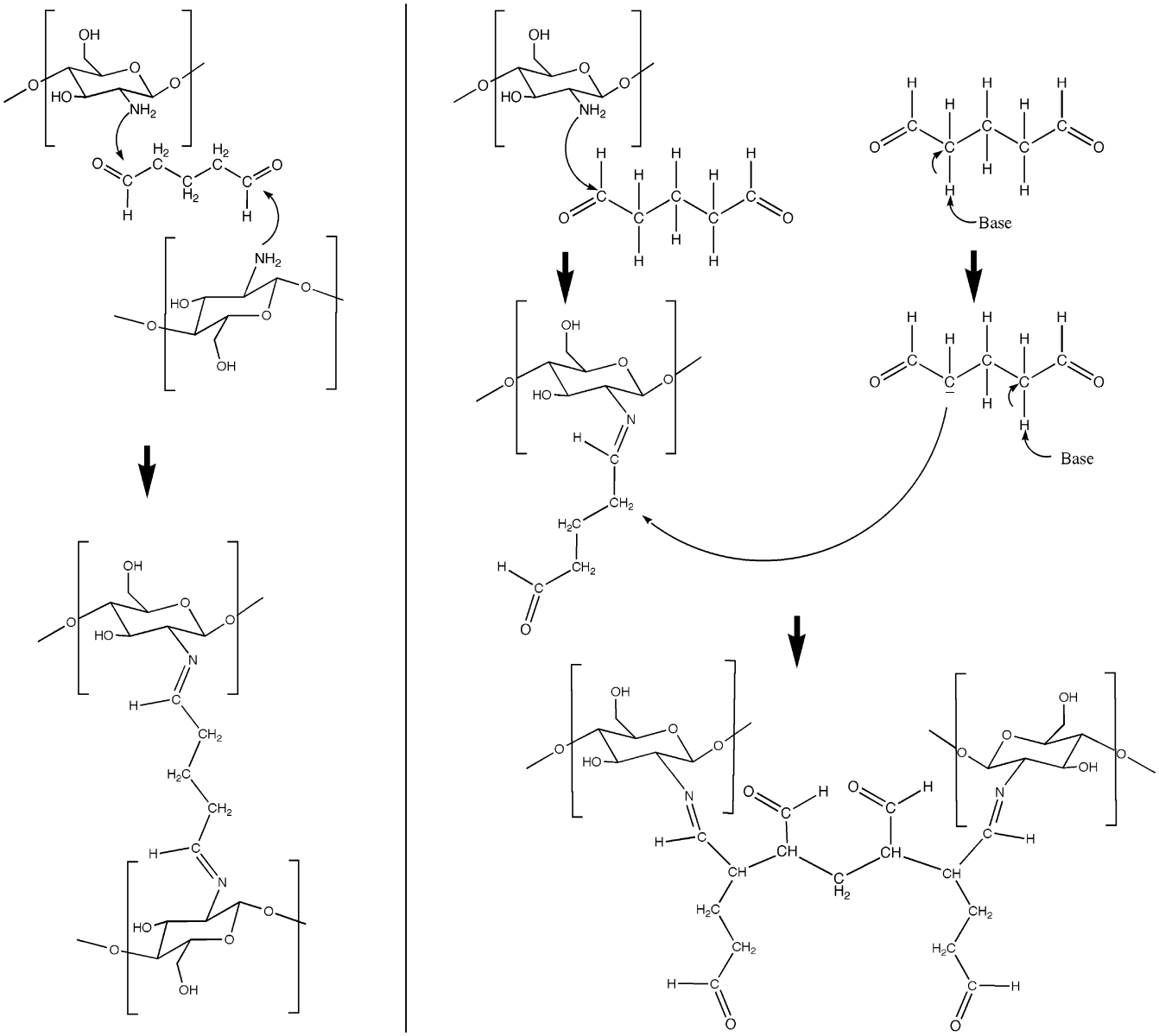

compared electrospun chitosan/poly(vinyl alcohol) (PVA) to purified chitosan10/trifluoroacetic acid. They observed bead-free electrospun fibers by adding an organic solvent, dichloromethane.

In this paper, randomly oriented fiber mats composed of continuous, bead-free fibers were electrospun from chitosan dissolved in trifluoroacetic acid (TFA). Four varieties of chitosan including low, medium, and high molecular weight and practical grade were spun. No purification of the chitosan nor additional polymers or solvents were used. Since the as-spun fibers dissolved in water, cross-linking the chitosan fibers is an integral step toward developing devices such as filters that would require a biodegradable, antimicrobial, porous nanofibrous mat that would be insoluble in water. Hence, a novel cross-linking method was identified utilizing vapor-phase GA. The viscosities of the chitosan/TFA solutions were measured and fiber mats were electrospun. Some of the electrospun fibers were then cross-linked with GA in a vapor chamber. The resultant GA cross-linked and the original as-spun nanofibrous mats were analyzed by scanning electron microscopy (SEM), Fourier transform infrared spectroscopy (FTIR), and microtensile testing, and their solubility was evaluated.

Materials and Methods

All compounds were used as received. Low and high molecular weight (MW) chitosan were purchased from Fluka (Switzerland). Glutaraldehyde (GA), 97% pure sodium hydroxide (NaOH), 99.7+ ACS. reagent-grade acetic acid, ReagentPlus 99% trifluoroacetic acid (TFA), and medium MW and practical-grade chitosan were purchased from Sigma−Aldrich (St Louis, MO). Room-temperature ultrapure water (Millipore QPAK system) was used to make the solubility test solutions.

Solution Preparation. Four different 2.7% (w/v) chitosan/TFA solutions were prepared with low (70 000), medium (∼190 000−310 000), and high molecular weight (MW) (500 000−700 000) as well as practical-grade (∼190 000−>375 000) chitosan. Solutions were mixed for at least 24 h on an Arma-Rotator A-1 (Bethesda, MD).

Electrospinning. The experimental electrospinning schematic is displayed in Figure 1. After a 5 mL Luer-Lok Tip syringe (Becton Dickinson & Co, Franklin Lakes, NJ) was repeatedly rinsed with TFA,

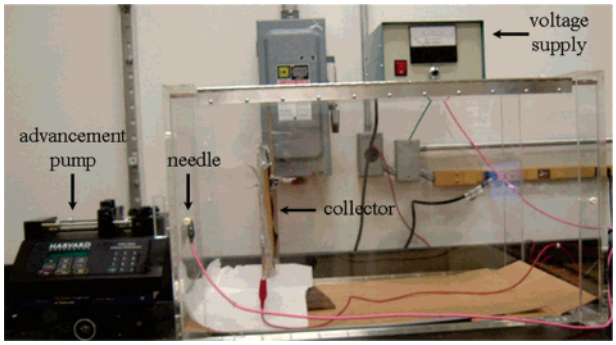

Figure 1. Experimental electrospinning setup.

4 mL of 2.7% (w/v) chitosan solution was loaded into the syringe and a Precision Glide 21-gauge needle (Becton Dickinson & Co, Franklin Lakes, NJ) was attached. By use of an alligator clip, the positive electrode of a high-voltage supply (Gamma High Voltage Research Inc., Ormond Beach, FL) was directly connected to the needle. The syringe was then placed on an advancement pump (Harvard Apparatus, Plymouth Meeting, PA), which was at a fixed distance of 6.4 cm from the negative electrode that was clipped to a copper plate wrapped in aluminum foil. Approximately 26 kV was then applied between the positive and the negative anodes as the solution was advanced at a rate of 1.2 mL/h. The temperature (degrees Celsius) and percent humidity in the laboratory during electrospinning were monitored by a digital thermohygrometer (Fisher Scientific, Pittsburgh, PA).

Viscometry. The viscosities of the chitosan/TFA solutions that were successfully electrospun were determined on a Brookfield digital viscometer, model HTBD (Stoughton, MA), with the SC4-27 link hanging spindle rotating at 100 rpm. All viscosity experiments were conducted at room temperature (23 °C).

Cross-Linking. The electrospun fibrous mats were placed in a 11.43 cm × 7.62 cm × 5.08 cm vapor chamber (VWR Scientific Products, Bridgeport, NJ) containing 4 mL of GA liquid. The GA liquid vaporized when it warmed to room temperature (23 °C) and was allowed to cross-link the fibers for at least 24 h.

Scanning Electron Microscope. Images of the electrospun fiber mats were obtained before and after cross-linking with a Zeiss Supra 50/VP field emission scanning electron microscope (FESEM). Some imaging of as-spun chitosan fiber mats that exhibited branching was conducted by use of a FEI/Phillips XL30 field emission environmental scanning electron microscope (FEESEM). A Denton vacuum desk II sputtering machine was utilized to coat the samples for 40 s with platinum. Average fiber diameter of the as-spun and cross-linked chitosan mats were obtained by use of the FESEM, by measuring 50 random fibers for each chitosan solution electrospun. Additional images after the mechanical testing was completed were taken of both the as-spun and cross-linked fibers close to their incident break face with the FESEM.

Fourier Transform Infrared Spectroscopy. Infrared spectra for the electrospun chitosan fiber mats before and after cross-linking were measured on an attenuated reflectance Fourier transform (Excalibur FTS-3000) spectrometer. Transmission mode with KBr pellets was utilized for all raw bulk chitosan samples. All spectra were taken in the spectral range of 4000−500 cm^{-1} by accumulation of 64 scans and with a resolution of 4 cm^{-1}.

Solubility. Decreased solubility of the chitosan nanofibers due to cross-linking with vapor GA was tested by subjecting as-spun and cross-linked medium MW chitosan mats to basic, acidic, and aqueous solutions. Six 15-mm^2 petri dishes (Becton Dickinson, Franklin Lakes, NJ), each containing 30 mL of solution, were utilized: three to test the as-spun fiber mats and three for the cross-linked fiber mats. Basic solution was 1 M NaOH, acidic solution was 1 M acetic acid, and aqueous solution was ultrapure water. Two samples, 2.54 cm × 1.27 cm cross-linked or as-spun fibrous mats were placed into each solution. After 15 min, if possible, one of the mats was removed, while the other remained in the solution for 72 h. The solubility and integrity of the mats over the time elapsed was visually inspected.

Uniaxial Tensile Tests. A tabletop uniaxial testing machine (Kawabata KES-G1 microtensile tester) was utilized to compare some mechanical properties of electrospun fibrous mats before and after cross-linking. Six fibrous mats (5.0 cm × 0.5 cm) were cut from medium MW chitosan electrospun mats. Three of the samples were cross-linked with GA vapor. All samples were mounted in C-shaped holders that were cut prior to the application of a strain rate of 0.02 s^{-1}. The testing was conducted at room temperature (23 °C). Young's modulus (megapascals), ultimate break strain, and ultimate tensile strength (megapascals) were calculated from the microtensile testing data as previously calculated by Lam.[34] All raw data acquired from the tensile test samples were normalized by accounting for the individual area density of each sample tested.

Results and Discussion

Viscometry. Using the appropriate molecular weight polymer conjoined with idealizing the viscosity of the polymer solution is an imperative step toward electrospinning. Normally, the higher of two molecular weight polymers dissolved in a solvent will result in higher viscosity.[35] While the viscosity of the four chitosan/TFA solutions varied, they all were found to successfully yield fibers. The viscosity (Table 1) of the low and medium MW chitosan solutions was found to be 168 and 1116 cP, respectively. The high MW and the practical-grade chitosan were determined to have the same viscosity: 308 cP. All solutions tested were 2.7% (w/v), which were created and tested in triplicate during the same testing session over which lab temperature and ambient humidity remained constant. Since these variables were all held constant, it is unclear at this time why the medium MW chitosan solutions demonstrated such an elevated viscosity in comparison to the other solutions tested. As noted in the FTIR section, the percent deacetylation was found to be ∼10% higher for the medium MW chitosan than for the others. The source of the chitin from which the chitosan has been derived from remains unknown for all bulk chitosan processed. We speculate that this variability was due to the intrinsic differences including the multitude of chain entanglements and conformations within the chitosan. Since all four solutions successfully yielded electrospun nanofibers, these data have been included as insight as to what the appropriate viscosity for electrospinning chitosan/TFA systems is.

Scanning Electron Microscopy. All chitosan/TFA solutions produced fine, cylindrical, continuous, and randomly oriented fibers. Figure 2 displays SEM micrographs of the various as-spun electrospun chitosan fibers including low MW (top left), medium MW (top right), high MW (bottom left), and practical grade (bottom right). Average fiber diameter size was determined by averaging the diameter of 50 random fibers; the smallest and largest diameter measurement were included in this average. Average fiber diameter (Table 1) increased as the MW increased for the low, medium, and high MW chitosan and were found to be 74 ± 28, 77 ± 29, and 108 ± 42 nm, respectively. While the MW of practical-grade chitosan was comparable to that of the medium MW chitosan, fibers electrospun from the practical-grade chitosan solution had the smallest average diameter size of 58 ± 20 nm. An explanation for this is currently unclear. It is possible that the practical-grade chitosan contains foreign contaminants that are interacting differently than the other chitosans. To define the range of diameters observed, the smallest and largest diameters measured for the various electrospun fibers are quoted. The smallest and largest fiber diameters measured were 37 and 170 nm for low

Table 1. Properties of Various Chitosans

	low MW chitosan	medium MW chitosan	high MW chitosan	practical-grade chitosan
molecular weight	70K	~190−310K	500−700K	190−>375K
percent deacetylation (%)	74	83	72	75
viscosity (cP)	168	1116	308	308
avg as-spun fiber diameter (nm)	74 ± 28	77 ± 29	108 ± 42	58 ± 20
avg cross-linked fiber diameter (nm)	387 ± 183	172 ± 75	137 ± 59	261 ± 160
diameter incr. due to cross-linking (%)	423	123	26.9	350

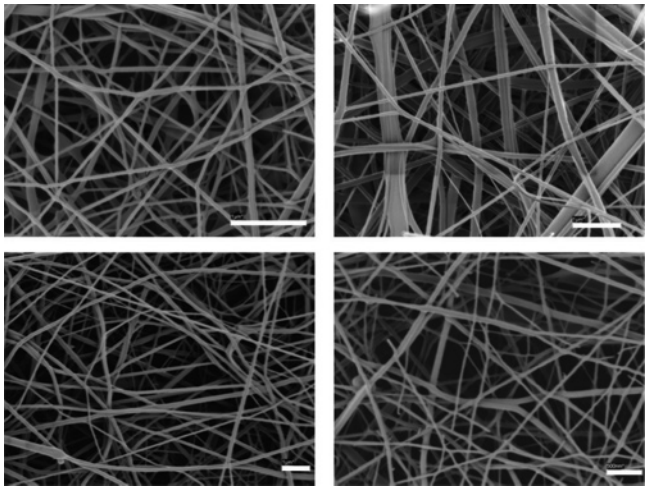

Figure 2. SEM images of electrospun chitosan fibers: low MW with 1 μm marker (top left), medium MW with 1 μm marker (top right), high MW with 1 μm marker (bottom left), and practical grade with 500 nm marker (bottom right). Images were taken on the FESEM.

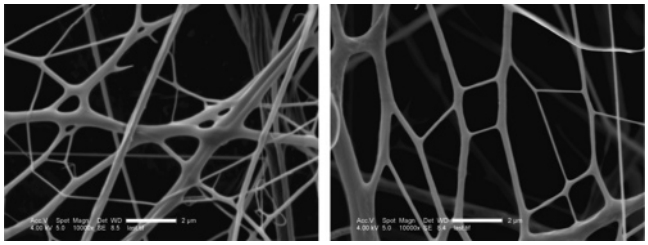

Figure 3. SEM images displaying branched morphology of electrospun mats composed of low MW chitosan with 2 μm marker (left) and practical-grade chitosan with 2 μm marker (right). Images were taken on the FEESEM.

MW, 31 and 174 nm for medium MW, 45 and 226 nm for high MW, and 28 and 120 nm for practical-grade chitosan. These diameter measurements also include the required sputter-coated layer of platinum (approximately 5−10 nm) that is applied prior to viewing the fiber diameters.

In our experiment, as evident in Figure 3, branching sometimes occurred in the low MW (left image) and the practical-grade (right image) chitosan mats. (The split fiber that is apparent in the low MW SEM image is a result of beam burning; the original fiber was continuous.) In order for ideal nonbranched fibers to be electrospun, an appropriate level of competition between electrical forces and surface tension must be maintained. Alterations from this state can result from elongations of the jet or evaporation of solvent, which can cause jet splitting[36] that consequently results in the branching of fibers. Previously, Zhao et al.[37] attributed this phenomena, which they observed in their lower MW samples to the presence of nonuniformly dispersed charges and molecular weight. Our finding parallels that of Zhao et al.: the low MW fibers exhibited some branching, which was possibly due to the intrinsically low MW of the bulk chitosan. Practical-grade chitosan resulted in

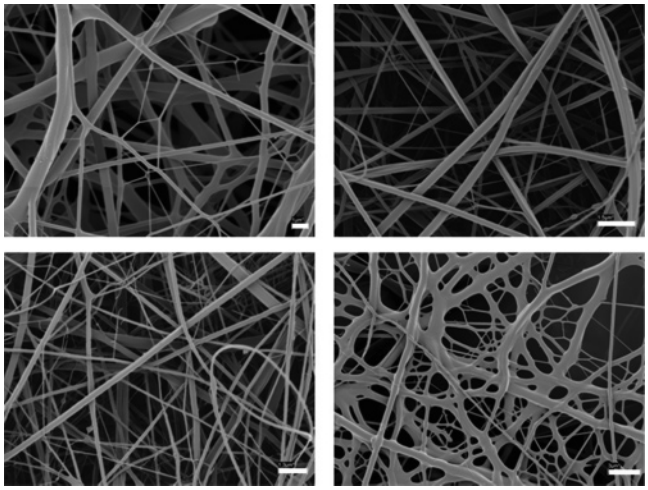

Figure 4. SEM image of GA cross-linked electrospun chitosan fibers: low MW with 1 μm marker (top left), medium MW with 1 μm marker (top right), high MW with 1.3 μm marker (bottom left), and practical grade with 3 μm marker (bottom right). Images were taken on the FESEM.

branching, which might be attributed to the nonuniformity of the raw material; it is known that practical-grade chitosan may contain foreign matter. This nonuniformity leads to branching because as the polymer solution is advanced, the electrostatic repulsion forces overcome the surface tension at the tip of the needle in some locations (where foreign matter is located). As previously noted, the competition between these two forces is a delicate balance that must be maintained to guarantee the production of ideal fibers.

An alternative reason why this branching might have occurred is due to the environment in which the fibers were electrospun instead of the bulk chitosan being at fault. While all chitosan fibers were created at approximately the same temperature (20−25 °C), there was a large discrepancy in the percent humidity that was measured. The fibers that exhibit branching (Figure 3) were created in the 20−25% humidity range while the fibers that did not exhibit this morphology (Figure 2) were spun when the humidity was twice as high, 40−45% humidity. It is possible that branching did not occur when the humidity level was elevated because solvent evaporation, due to the excess moisture levels in the air, occurred at a slower rate. In the future, creating an atmosphere within the electrospinning apparatus that will hold both the temperature and humidity constant will be further investigated.

To cross-link the as-spun chitosan fiber mats, they were placed in a vapor chamber with GA vapor. Figure 4 displays SEM images of GA-cross-linked electrospun chitosan fibers from low (top left), medium (top right), and high MW (bottom left), as well as practical-grade (bottom right) chitosan. From all of the SEM images, it is evident that after cross-linking the fiber mats retain their integrity as long, randomly oriented, cylindrical fibers. However, from the SEM images whether the GA vapor has coated or penetrated into the fibers is unclear. It

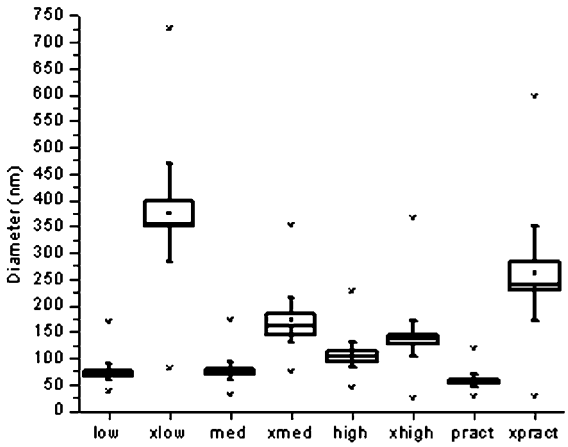

Figure 5. Box plots displaying the diameter size distribution of fiber diameters for the various electrospun chitosans: from left to right, low MW, cross-linked low MW, medium MW, cross-linked medium MW, high MW, cross-linked high MW, practical grade, and cross-linked practical grade. The box outline is the standard error, the square inside the box is the mean data point, the line inside the box is the median data location, the whiskers display the upper inner and lower inner fence values.Above and below the whiskers: (+) max/min data point; (×) first/99th percentile.

is not known if cross-linking is occurring within individual fibers and/or if it is occurring between adjacent touching fibers. FTIR results discussed later reveal the mechanism by which the cross-linking occurred, while mechanical testing, also discussed later, revealed that cross-linking might be fusing the fibers together and causing the mechanical changes associated with this. Still, none of the aforementioned analyses reveal how deep the cross-linker penetrated into the fibers. Future planned studies utilizing atomic force microscopy (AFM) along various parts of the fiber mat such as along the length of individual fibers, at fiber−fiber intersections, and perpendicular to a fiber diameter will be more revealing.

Again, it is important to note that the cross-linked low MW and practical-grade chitosan fiber mats in these images were spun in the lower humidity range, which could attest to the presence of branching. A few white spots that are observed in the image of the medium MW chitosan fibers are most likely the result of an agglomeration of GA and are not electrosprayed droplets of polymer. Average fiber diameters for the cross-linked chitosan fibers for the low, medium, and high MW and practical-grade chitosan were found to be 387 ± 183, 172 ± 75, 137 ± 59, and 261 ± 160 nm, respectively (Table 1). The smallest and largest fiber diameters measured were 80 and 725 nm for low MW, 76 and 353 nm for medium MW, 23 and 365 nm for high MW, and 26 and 596 nm for practical-grade chitosan. Generally, the smaller as-spun fibers experienced a higher increase in average diameter upon cross-linking. This could possibly be a result of their higher ratio of surface area to volume. Additionally, as the GA cross-links the chitosan as illustrated in Scheme 1, spreading of the molecules occurs.

Figure 5 displays a box plot of the fiber size distributions for both the as-spun and cross-linked electrospun chitosan fibers. The box outline is the standard error, the square inside the box is the mean data point, the line inside the box is the median data location, and the whiskers display the upper inner and lower inner fence values. Above and below the whiskers, + indicates the max/min data point and × indicates the first/99th percentile (these values appear to overlap in the figure). The upper inner fence whisker extends to the 75th percentile plus 1.5 times the interquartile range, while the lower inner fence value extends down to the 25th percentile minus 1.5 times the interquartile

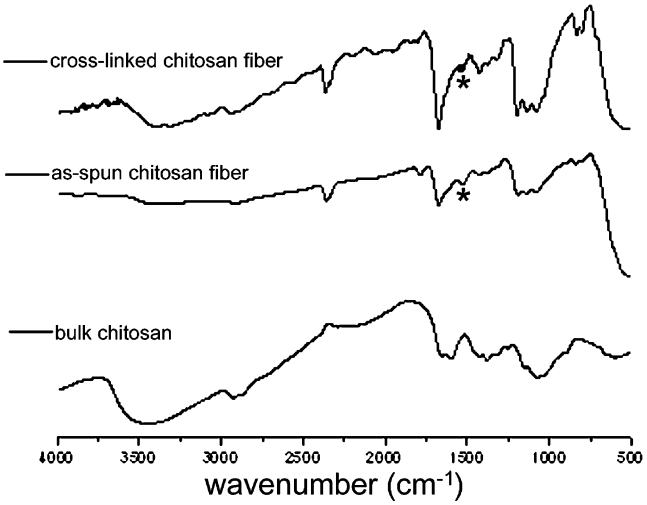

Figure 6. FTIR spectra of cross-linked electrospun medium MW chitosan fibers (top), electrospun medium MW chitosan fibers (middle), and bulk sample of medium MW chitosan (bottom).

range. Data points that lie outside the fence values are considered outliers. Outliers and individual data points were not plotted on the provided graph. Since the as-spun fibers are next to their cross-linked counterparts, it is apparent that most of the data points for the vapor−cross-linked fibers are greater than their as-spun chitosan nanofibers.

Fourier Transform Infrared Spectroscopy. FTIR spectra were taken of the bulk chitosan samples and of the electrospun mats before and after cross-linking with GA. Figure 6 displays the spectra of the medium MW chitosan in bulk, electrospun fiber form, and cross-linked electrospun fiber form. By use of a combination of the OH stretching band at 3450 cm^{-1}, amide I bands at 1655 and 1630 cm^{-1}, amide II band at 1560 cm^{-1}, C−H stretching band at 2877 cm^{-1}, the bridge oxygen stretching band at 1160 cm^{-1}, and the C−O stretching bands at 1070 and 1030 cm^{-1}, the percent deacetylation can be determined.[38] Current literature provides seven different peak ratios (1560/1070, 1560/1030, 1630/2878, 1655 + 1630/2878, 1550/2878, 1655/3450, and 1655/2867) that have been investigated to determine the percent deacetylation of chitosan. Additionally, Roberts and co-workers[39] and Miya and co-workers[40] each utilized their own alternative methods of baseline correction used for peak height analysis. Generally, the greatest source of error when calculating percent deacetylation via FTIR is from bulk water, which can provide up to 1% error even in well-dried samples.

With the work of Shigemasa et al.[38] as a foundation, the 1560/1070 peak ratio was used to determine the percent deacetylation of the bulk chitosan samples. On the basis of the FTIR spectra of the bulk chitosan materials, the low MW chitosan was 74%, the medium MW was 83%, the high MW was 72%, and the practical grade was 75% deacetylated.

The FTIR spectra of the as-spun and cross-linked chitosan fiber samples were evaluated by attenuated reflectance FTIR; the whole fibers were analyzed directly. Of importance for the spectra of the as-spun chitosan fibers was the presence of trifluoroacetic acid that was used to electrospin the chitosan; the peak at 1750 cm^{-1} indicated the presence of a carboxylic acid.

As a result of the cross-linking reaction, significant changes are observed in the FTIR spectra of the as-spun versus the cross-linked electrospun fibers. The FTIR spectra of cross-linked chitosan fibers displayed a distinct change in the carbonyl-amide

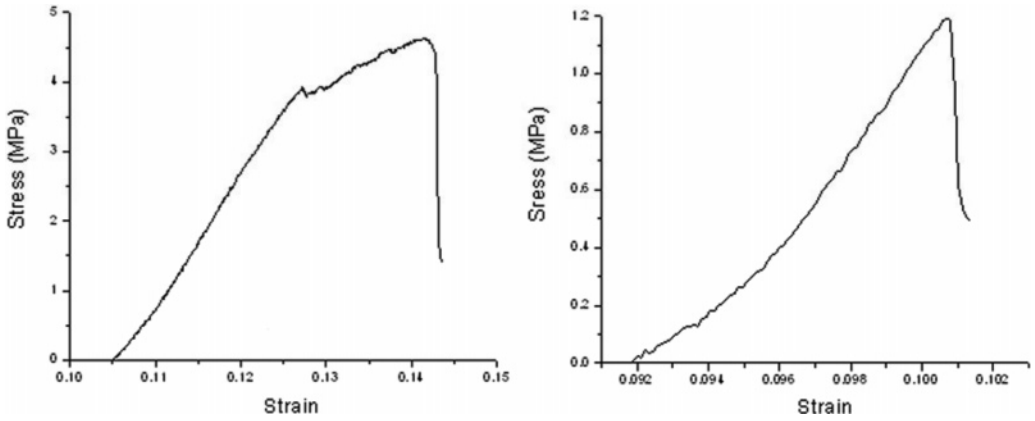

Figure 7. Stress−strain curve of electrospun medium MW chitosan mat (left) and cross-linked electrospun medium MW mat (right).

region. The primary amine peak decreased when the chitosan fibers were cross-linked, while a new peak for C═N imine appeared. According to the literature, the C═N peak can be anywhere from 1620 to 1660 cm^{-1}.[21] This appeared as a strong split peak at 1650 cm^{-1}. The peak at 1560 cm^{-1} (shown by asterisks in Figure 6) disappeared in the cross-linked chitosan fibers due to the loss of the free amines, indicating that the fiber mats exhibited a Schiff base imine functionality that was also reported by Tual et al.[19] in their chitosan/GA film experiment. Our experiments exhibited the same color change that Tual observed; namely, our mats became yellow upon cross-linking (as-spun mats were white). Finally, to confirm that Michael-type cross-linking did not occur, we note that no identifiable carbonyl groups appear in the 1720−1730 cm^{-1} IR spectra.

Solubility. The as-spun and the cross-linked medium MW chitosan fibers were immersed in acetic acid, water, and NaOH solutions. When the as-spun fibers were subjected to acetic acid solution, they appeared to disintegrate instantaneously: the fibers dissolved and neither the mat nor individual fibers remained. The as-spun fiber mats dispersed instantly in the ultrapure water; there was no form retention. Upon looking very carefully in the water, cloudy white specks could be seen. Therefore, perhaps some agglomeration of nanofibers remained since an opaque white color was visible with the unaided eye. It is certain that the mat instantly broke apart upon interacting with water and could not be recovered. When subjected to the NaOH solution, the as-spun chitosan fiber mats survived. They remained white and a rectangular shape for both the 15 min and the 72 h test.

The cross-linked chitosan fiber mats behaved in a different manner from the as-spun mats; they survived the acetic acid, ultrapure water, and NaOH solutions for 15 min. Additionally, after 72 h the fiber mats looked the same; their rectangular shape and yellow color were retained. After the cross-linked chitosan fiber mats were removed from the solutions, visual inspection implies that their shape and rigidity remained unaltered.

Mechanical Testing. The mechanical properties of both the as-spun and cross-linked randomly oriented chitosan fibrous mats were determined on a Kawabata microtensile tester; the findings were supported by the subsequently provided SEM images. Figure 7 displays a typical stress−strain plot for both the as-spun (Figure 7, left) and cross-linked (Figure 7, right) electrospun medium MW chitosan fibers. The average Young's modulus (tensile elastic modulus) of the chitosan mats were determined from the slope of the linear elastic region of the stress−strain curve and averaged among the samples. The Young's modulus (Table 2) of the as-spun and cross-linked fibers was found to be 154.9 ± 40.0 and 150.8 ± 43.6 MPa, respectively. The initial steep slope of the curves corresponds to the nanofibers' intrinsically high cohesive forces due to the large number of fiber-to-fiber contacts; therefore, the nanofibrous mats have a high resistance to deformation.[34]

Table 2. Mechanical Property Data of Electrospun As-Spun and Cross-Linked Medium MW Chitosan

	as-spun fibers	cross-linked fibers
Young's modulus (MPa)	154.9 ± 40.0	150.8 ± 43.6
break strain	0.12 ± 0.03	0.10 ± (8.49×10^{-5})
ultimate tensile strength (MPa)	4.07 ± 0.80	1.19 ± 0.0041

A pseudo-yield point is present in the as-spun fibers stress−strain plot as evident by the second portion of the increasing slope that increases at a reduced rate. Hence, a reduced increase in modulus is observed, which corresponds to fiber alignment along the tensile pull axis. As the once randomly aligned fibers are being aligned, there is an increase in the allowable stresses until the break strain and ultimate tensile strength are achieved; they average (Table 2) 0.12 ± 0.03 and 4.07 ± 0.80 MPa, respectively, for the as-spun medium MW chitosan fibers.

The graph of the cross-linked medium MW fibers does not display the same pseudo-yield point but features a distinct maximum where the break occurred during tensile pulling. This loss might be indicative that the individual fibers have become locked together and therefore cannot slip past each other as demonstrated by the as-spun fibrous mats. The cross-linked medium MW fibers have a lower average break strain (Table 2) of 0.10 ± (8.49×10^{-5}) and additionally a decreased ultimate tensile strength of 1.19 ± 0.0041 MPa in comparison with the as-spun fibers. No mechanical data have been reported on electrospun chitosan or chitosan/polymer nanofibers or nanofibrous mats. Mechanical properties of chitosan fibers created by traditional techniques such as wet-spinning have been evaluated.[14,41,42] Knaul et al.[21] mechanically tested wet-spun chitosan fibers with various concentrations of GA cross-linker. They found that modulus, break, and tenacity decreased while brittleness increased after a particular amount of cross-linking agent was employed. Thus, they proposed that the dialdehyde degrades the molecular structure at high concentrations of GA or that stress concentrations might form within the fibers. In our next set of experiments we plan on evaluating the time dependences that cross-linking with GA vapor has on chitosan nanofibers.

The previously described distinct difference in the elasticity of the as-spun versus cross-linked fibers can be supported by the SEM images (Figure 8). These images were taken in close proximity to the failure point of the fiber mats so that changes in individual fiber morphology could be observed. Figure 8 (top

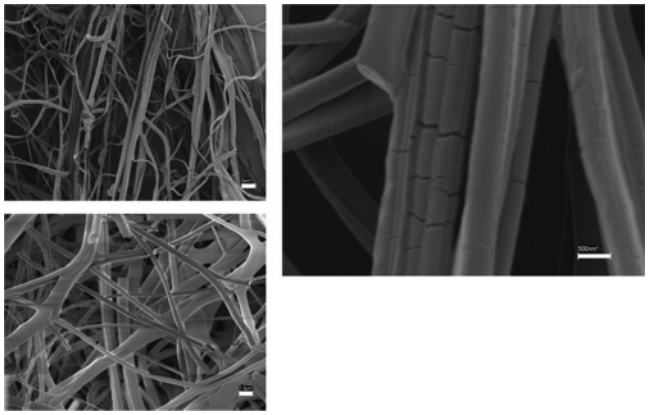

Figure 8. SEM images of electrospun chitosan fibers after mechanical testing close to their breaking point: overall alignment of as-spun medium MW chitosan fibers with 3 μm marker (upper left); overall structure of cross-linked medium MW chitosan fibers with 1.3 μm marker (lower left); close-up of as-spun medium MW chitosan fibers with 500 nm marker (right). Images were taken on the FESEM.

left) displays an image of as-spun fibers after mechanical testing that contains both aligned fibers and a multitude of cracks or locations where extensions occurred on the fibers prior to their ultimately breaking. The zoomed-in image, Figure 8 (right), displays cracks that propagated perpendicular to the long axis of the fiber. This phenomenon shows the elastic nature of the as-spun fibers. The lower left image in Figure 8 exhibits that the cross-linked fiber mats retained their randomly oriented fiber composition and experienced a multitude of broken fibers prior to their ultimate break. Cross-linked fibers did not demonstrate alignment or elongation prior to their failure; it can be concluded that they act less elastically than the as-spun chitosan nanofibers.

Conclusion

Fibrous mats were successfully electrospun from low, medium, and high molecular weight as well as practical-grade chitosan. The high MW and practical-grade chitosan solutions were experimentally found to have the same viscosity: 308 cP. The low and medium MW chitosan/TFA solutions were found to have viscosities of 168 and 1116 cP, respectively. As noted, there was found to be only a minimal correlation between viscosity and fiber diameter; these data have been included to provide insight concerning the required viscosity to electrospin chitosan/TFA successfully rather than supplying information about general electrospinning parameters, fiber production, or relationship to mechanical properties.

All chitosans were capable of being electrospun into fiber mats without exhibiting any branching. Occasionally, the low MW and practical-grade chitosan fibers displayed branching; it is unclear at this time whether this is due to the bulk material, percent humidity, or both of these conditions. We plan to investigate fully the role of humidity when electrospinning our chitosan/TFA solutions to answer this question.

From the data collected on the average fiber diameter of as-spun and cross-linked chitosan fibers, it can be concluded that vapor cross-linking increases the average fiber diameter by a measurable amount, which is most likely due to the GA bonding to the chitosan and thus stretching the molecules. The average amount that the average fiber diameter increased after cross-linking was 161 nm. Additionally, it is of interest to note that the average diameter sizes for the low, medium, and high MW and practical-grade chitosan fibers were found to be 74 ± 28, 77 ± 29, 108 ± 42, and 58 ± 20 nm. Therefore, on average the low and medium MW as well as the practical-grade electrospun chitosan fibers were truly in the nano regime.

The most accurate method of calculating the percent deacetylation of bulk chitosan utilizing FTIR spectra was by using the 1560/1070 peak ratio. By use of this peak ratio, it was determined that the bulk low MW chitosan was 74%, medium MW chitosan was 83%, high MW chitosan was 72%, and practical-grade chitosan was 75% deacetylated. FTIR confirmed that cross-linking the chitosan fibers with GA occurred, as evident by the shift in the ratio of peaks from 1650 to 1560 cm^{-1} in the carbonyl-amide region, indicating that Schiff base imine functionality occurred.

Cross-linking with GA vapor made the medium MW chitosan fiber mats insoluble in NaOH, acetic acid, and ultrapure water solutions for at least 72 h. Upon removal of the fibrous mats from these solutions, their color as well as their rectangular shape was maintained.

Uniaxial tensile testing indicated that once chitosan fiber mats are cross-linked with GA, they lose some of their elastic properties and become more brittle. All tested mechanical properties were found to decrease after cross-linking. The Young's modulus of the cross-linked fiber mats was found to be 4.1 MPa lower, the average break strain was found to be 0.02 lower, and the ultimate tensile strength was determined to be 2.88 MPa lower than those of the as-spun nanofiber mats.

The decreasing slope prior to the ultimate failure of the as-spun fiber mats indicates that these fibers experienced a reduced increase of mechanical properties prior to their breaking point. This can be attested to the lessening influence of cohesive forces (from the fiber−fiber contacts) and replacement with fiber alignment and pulling. Additionally, the SEM images confirm that the as-spun fibers developed cracks perpendicular to the length of the fibers that allowed the fibers to elongate. Alternatively, the cross-linked fibers did not experience a slow degradation of properties but rather a quick break, as supported by the SEM images of sharply broken fibers. The cross-linker effectively locked the chitosan fibers together, thus prohibiting fiber slippage and causing the loss of the pseudo-yield point.

In conclusion, we have electrospun bead-free, continuous, randomly oriented nanofibrous mats from various molecular weights (low, medium, and high) and a practical grade of chitosan. Questions remain as to whether the GA vapor is penetrating fully into the chitosan fibers, coating individual fibers, or concentrating at fiber−fiber contacts during the cross-linking process. Based upon the differences in solubility and mechanical properties, as supported by the SEM images of the as-spun versus cross-linked chitosan fiber mats, our next research initiative is to determine the optimal exposure time of the chitosan fiber mats to the GA vapor. We believe that the current exposure time of the mats to the GA vapor is longer than ideal and that by decreasing and optimizing this time factor we will find an increase in mechanical properties, while retaining the decreased solubility.

Acknowledgment. We thank Milind Gandhi and Dr. Frank Ko for their help and use of the Kawabata microtensile tester. SEM imaging would not have been possible without the use of the Drexel University Materials Characterization Facility including Aaron Sakulich's assistance. Also, thanks to Ya Liang and Dr. Giuseppe Palmese for access and assistance on their Brookfield digital viscometer. This work was funded in part by NSF IGERT (DGE-0221664) and by the Department of Health for the Commonwealth of Pennsylvania.

References and Notes

(1) Kumar, M. N. V. R. *React. Funct. Polym.* **2000**, *46* (1), 1−27.
(2) Pillai, O.; Panchagnula, R. *Curr. Opin. Chem. Biol.* **2001**, *5* (4), 447−451.
(3) Dodane, V.; Vilivalam, V. D. *Pharm. Sci. Technol. Today* **1998**, *1* (6), 246−253.
(4) Vartiainen, J.; Motion, R.; Kulomen, H.; Ratto, M.; Skytta, E.; Ahvenainen, R. *J. Appl. Polym. Sci.* **2004**, *94*, 986−993.
(5) Berger, J.; Reist, M.; Mayer, J. M.; Felt, O.; Peppas, N. A.; Gurny, R. *Eur. J. Pharm. Biopharm.* **2004**, *57*, 19−34.
(6) Khor, E.; Lim, L. Y. *Biomaterials* **2003**, *24* (13), 2339−2349.
(7) Yang, J. M.; Lin, H. T. *J. Membr. Sci.* **2004**, *243*, 1−7.
(8) Chirkov, S. N. *Appl. Biochem. Microbiol.* **2002**, *38* (1), 1−8.
(9) Shahidi, F.; Arachchi, J. K. V.; Jeon, Y.-J. *Trends Food Sci. Technol.* **1999**, *10* (2), 37−51.
(10) Stephen, A. M. *Food Polysaccharides and Their Applications*; Marcel Dekker: New York, 1995; p 672.
(11) Hwang, J. K.; Shin, H. H. *Korea−Aust. Rheol. J.* **2000**, *12* (3/4), 175−179.
(12) Ligler, F. S.; Lingerfelt, B. M.; Price, R. P.; Schoen, P. E. *Langmuir* **2001**, *17* (16), 5082−5084.
(13) Schauer, C. L.; Chen, M.-S.; Chatterley, M.; Eisemann, K.; Welsh, E. R.; Price, R. R.; Schoen, P. E.; Ligler, F. S. *Thin Solid Films* **2003**, *434* (1−2), 250−257.
(14) Wei, Y. C.; Hudson, S. M.; Mayer, J. M.; Kaplan, D. L. *J. Polym. Sci., Part A: Polym. Chem.* **1992**, *30* (10), 2187−2193.
(15) Jin, J.; Song, M.; Hourston, D. J. *Biomacromolecules* **2004**, *5* (1), 162−168.
(16) Welsh, E. R.; Schauer, C. L.; Qadri, S. B.; Price, R. R. *Biomacromolecules* **2002**, *3* (6), 1370−1374.
(17) Welsh, E. R.; Schauer, C. L.; Santos, J. P.; Price, R. R. *Langmuir* **2004**, *20* (5), 1807−1811.
(18) Jameela, S. R.; Jayakrishnan, A. *Biomaterials* **1995**, *16* (10), 769−775.
(19) Tual, C.; Espuche, E.; Escoubes, M.; Domard, A. *J. Polym. Sci., Part B: Polym. Phys.* **2000**, *38* (11), 1521−1529.
(20) Tomihata, K.; Ikada, Y. *J. Polym. Sci., Part A: Polym. Chem.* **1997**, *35* (16), 3553−3559.
(21) Knaul, J. Z.; Hudson, S. M.; Creber, K. A. M. *J. Polym. Sci., Part B: Polym. Phys.* **1999**, *37* (11), 1079−1094.
(22) Muzzarelli, R. A. A. *Chitin*; Pergamon: Oxford, U.K., 1977; p 309.
(23) Koyama, Y.; Taniguchi, A. *J. Appl. Polym. Sci.* **1986**, *31* (6), 1951−1954.
(24) Roberts, G. A. F.; Taylor, K. E. *Makromol. Chem.* **1989**, *190* (5), 951−960.
(25) Rutledge, G. C.; Shin, M. Y.; Warner, S. B.; Buer, A.; Grimler, M.; Ugbolue, S. C. *A Fundamental Investigation of the Formation and Properties of Electrospun Fibers*; University of Massachusetts Dartmouth and Massachusetts Institute of Technology: Cambridge, MA,1999; pp 1−10.
(26) Kim, J. S.; Lee, D. S. *J. Polym. Sci.* **2000**, *32* (7), 616−618.
(27) Huang, Z.-M.; Zhang, Y. Z.; Kotaki, M.; Ramakrishna, S. *Compos. Sci. Technol.* **2003**, *63* (15), 2223−2253.
(28) Duan, B.; Dong, C.; Yuan, X.; Yao, K. *J. Biomater. Sci., Polym. Ed.* **2004**, *15* (6), 797−811.
(29) Geng, X.; Kwon, O.-H.; Jang, J. *Biomaterials* **2005**, *26* (27), 5427−5432.
(30) Spasova, M.; Manolova, N.; Paneva, D.; Rashkov, I. *e-Polymers* **2004**, *56*, 1−12.
(31) Bhattarai, N.; Edmondson, D.; Veiseh, O.; Matsen, F. A.; Zhang, M. *Biomaterials* **2005**, *26*, 6176−6184.
(32) Min, B.-M.; Lee, S. W.; Lim, J. N.; You, Y.; Lee, T. S.; Kang, P. H.; Park, W. H. *Polymer* **2004**, *45*, 7137−7142.
(33) Ohkawa, K.; Cha, D.; Kim, H.; Nishida, A.; Yamamoto, H. *Macromol. Rapid Commun.* **2004**, *25*, 1600−1605.
(34) Lam, H. L. Electrospinning of Single Wall Carbon Nanotube Reinforced Aligned Fibrils and Yarns. Drexel University, Philadelphia, PA, 2004.
(35) Ramakrishna, S.; Fujihara, K.; Teo, W.-E.; Lim, T.-C.; Ma, Z. *An Introduction to Electrospinning and Nanofibers*; World Scientific: Singapore, 2005; p 382.
(36) Koombhongse, S.; Liu, W.; Reneker, D. H. *J. Polym. Sci., Part B: Polym. Phys.* **2001**, *39* (21), 2598−2606.
(37) Zhao, Y. Y.; Yang, Q. B.; Lu, X. F.; Wang, C.; Wei, Y. *J. Polym. Sci., Part B: Polym. Phys.* **2005**, *43* (16), 2190−2195.
(38) Shigemasa, Y.; Matsuura, H.; Sashiwa, H.; Saimoto, H. *Int. J. Biol. Macromol.* **1996**, *18* (3), 237−242.
(39) Miya, M.; Iwamoto, R.; Ohta, K. M. S. *Kobunshi Ronbunshu* **1985**, *42* (3), 181−189.
(40) Baxter, A.; Dillon, M.; Taylor, K. D. A.; Roberts, G. A. F. *Int. J. Biol. Macromol.* **1992**, *14*, 166−169.
(41) Knaul, J.; Hooper, M.; Chanyi, C.; Creber, K. A. M. *J. Appl. Polym. Sci.***1998**, *69* (7), 1435−1444.
(42) Knaul, J. Z.; Hudson, S. M.; Creber, K. A. M. *J. Appl. Polym. Sci.* **1999**, *72* (13), 1721−1732.

BM060804S